

pdftitle=Retrieval of Macrophysical Cloud Parameters from MIPAS: Algorithm and Validation pdfauthor=J. Hurley et al.

title Manuscript prepared for Atmos. Meas. Tech. Discuss.

with version 2.0 of the L^AT_EX class copernicus_discussions.cls.

Date: 13 October 2010

Retrieval of Macrophysical Cloud Parameters from MIPAS: Algorithm Description and Preliminary Validation

J. Hurley, A. Dudhia, and R. G. Grainger

Atmospheric, Oceanic and Planetary Physics, Clarendon Laboratory, Department of Physics,
Parks Road, Oxford

Correspondence to: J. Hurley
(hurley@atm.ox.ac.uk)

Abstract

abstr The Michelson Interferometer for Passive Atmospheric Sounding (MIPAS) onboard EN-
VISAT has the potential to be particularly useful for studying high, thin clouds, which have been
difficult to observe in the past. This paper details the development, implementation and test-
5 ing of an optimal-estimation-type retrieval for three macrophysical cloud parameters (cloud top
height, cloud top temperature and cloud extinction coefficient) from infrared spectra measured
by MIPAS, employing additional information derived to improve the choice of a priori. The
retrieval is applied and initially validated on MIPAS data. From application to MIPAS data, the
retrieved cloud top heights are assessed to be accurate to within 50 m, the cloud top temperatures
10 to within 0.5 K and extinction coefficients (along the limb path attributable (mostly) to clouds)
to within a factor of 15%, for clouds having extinction between 10^{-4} km^{-1} and 10^{-1} km^{-1} .
This algorithm has been adopted by the European Space Agency's 'MIPclouds' project, which
itself recognises the potential of MIPAS beyond monitoring atmospheric chemistry and seeks
to study clouds themselves rigorously using MIPAS.

1 Introduction

intro

Although much of atmospheric infrared remote sensing is based upon analysis of data to es-
timate constituent concentrations — where the presence of cloud particles in the measurements
is treated as a source of error — it is possible to isolate measurements of cloud in order to
20 determine the properties of clouds themselves. Clouds (especially high cloud such as cirrus)
represent one of the largest uncertainties in climate studies (Intergovernmental Panel on Cli-
mate Change, 2008) — and in order to have reliable estimates of radiative forcing and climatic
impact, accurate distributions of cloud frequencies and properties must be available. Satellite
instruments provide an opportunity to study the properties of clouds on a global scale.

1.1 Overview of MIPAS-ENVISAT

The Michelson Interferometer for Passive Atmospheric Sounding (MIPAS) is an infrared limb-viewing instrument and was launched in March 2002 on the European Space Agency's Environmental Satellite (ENVISAT) which, with large inclination on a polar orbit in conjunction with azimuth scanning, enables global coverage pole-to-pole. (European Space Agency, 2005)

MIPAS was designed to measure limb-emission spectra (primarily for trace gases such as CO₂ (used to retrieve pressure and temperature), O₃, H₂O, HNO₃, CH₄, N₂O and NO₂) at a high spectral resolution in the near- to mid-infrared from 685 cm⁻¹ to 2410 cm⁻¹. In its initial phase, MIPAS operated at a spectral sampling of 0.025 cm⁻¹, measuring spectra nominally every 3 km vertically in the troposphere — however following **persistent malfunctions in the smooth and consistent operation of the interferometer slide mechanism in early 2004**, the sampling was decreased to 0.0625 cm⁻¹ but the measurement frequency increased to nominally every 1.5 km **upward from the troposphere through the lower stratosphere (Mantovani, 2005). The MIPAS field-of-view is trapezoidal in the vertical, with a vertical extent varying between 3 – 4 km, depending upon definition. It has a characteristically wide horizontal field-of-view, extending approximately 200 km.**

1.2 Overview of Clouds from Satellites

Cloud properties fall loosely into two categories: macrophysical and microphysical. Macro-physical properties are the large-scale properties (ie. bulk or extent), such as the altitude of a cloud, the physical depth and extent of a cloud, or are basic thermodynamic quantities, such as the temperature at the cloud top or the temperature structure within the cloud body. Microphysical parameters are, by opposition, those which relate to the small-scale (ie. constituent particle) of the cloud — such as the size and shape of cloud particles, and their distribution (which is often described in terms of water content), thus including properties such as number density, and influencing cloud optical depth, albedo, emissivity and transmissivity. Cloud extinction is strictly a combination of macrophysical and microphysical parameters as it is derived from both the physical extent of the cloud, as well as its absorption and scattering characteristics. How-

ever, from the perspective of an assumed model whereby there is no scattering, and a single homogeneous extinction characterising the bulk of the cloud mass, in this study is designated as a macrophysical parameter.

Whilst most of our knowledge of the microphysical properties of clouds come from in-situ measurements, predominantly by aircraft-mounted instruments (campaigns include Weickmann (1947) over Germany, FIRE I and II over Wisconsin and Kansas (1992), SUCCESS over Oklahoma and Kansas (1996), CEPEX (1997), EUCREX over the Atlantic Ocean and mid-latitudes in Europe (2000), and CRYSTAL-FACE over Florida (2002)), satellite instruments are particularly well-suited to observing macrophysical parameters, not least because of the large-scale geographical regions they survey. As a general rule, limb-viewing instruments are competent at retrieving vertically-dependent parameters (such as cloud top height/pressure or cloud depth/extent) with great accuracy, although have poorer horizontal-resolving potential — but are able to detect even clouds having thin opacities of less than 0.01 due to the inherently long limb pathlength. On the contrary, nadir-viewing instruments suffer from poor vertical resolution when retrieving atmospheric temperature and composition from which cloud top temperatures (and hence cloud top heights/pressures) are derived, are limited to thicker clouds, but have very good horizontal resolution. Different spectral ranges are sensitive to different cloud properties: for instance, microwave instruments often are not sensitive to ice cloud particles (since such short wavelengths do not cause much scattering from typical ice particles, and are high-energy enough to pass through optically thin ice clouds unobstructed), whereas visible and infrared instruments are often limited to the first layer of cloud encountered and unable to measure below (as typical clouds will be opaque to radiation at these wavelengths) (e.g. ESA's Living Planet website, 2010) . It is thus important to choose to retrieve cloud properties appropriate to the satellite instrument's capabilities.

There have been many studies on clouds over the years producing climatologies: by Barton (1983), Warren et al. (1985), Woodbury and McCormick (1983), Prabhakara et al. (1988), Wylie and Menzel (1989), Wylie et al. (1994) — but these were all limited by a lack of global coverage. Currently, the Stratospheric Aerosol and Gas Experiment (SAGE) (e.g. SAGE-III-ATBD-Team, 2002), the High Resolution Infrared Radiation Sounder (HIRS) instrument (e.g.

Wylie et al., 2005), the International Satellite Cloud Climatology Project (ISCCP) (e.g. ISCCP, 2008) and the GRAPE project (e.g. Sayer et al., 2009) are actively compiling cloud climatologies. However, past and current cloud detection algorithms often miss much thin cloud in satellite measurements — and hence conventional cloud climatologies and inventories are in no way complete with respect to high thin cloud such as cirrus (Wylie et al., 2005). In fact, with the exception of SAGE, limb-viewing has not been used for cloud measurements since such instruments tend to target atmospheric composition for which cloud detection is the only requirement, and limb-viewing cloud campaigns tend to be experimental rather than operational, hence yielding only short-time-series over a limited geographical region. Given that MIPAS should be quite sensitive to high, thin cloud if an appropriate detection mechanism is employed, it is a natural candidate to contribute climatological information about these clouds.

Retrieval of cloud parameters from instruments such as MIPAS, although highly instrument-specific, are dependent upon cloud-detection algorithms as estimators of cloud location (cloud top height/pressure/depth), and as selectors of data upon which retrieval schemes are run. Generally, cloud detection methods for limb-viewing and solar occultation IR instruments (such as MIPAS) are based upon a

- *threshold on:* radiance (such as the Cryogenic Limb Array Etalon Spectrometer CLAES experiment (CLAES, 2007) and High Resolution Dynamics Limb Sounder HIRDLS (Lambert et al., 1999)), transmission (Atmospheric Trace Molecule Spectroscopy ATMOS experiment (Kahn et al., 2002)), extinction (Improved Stratospheric and Mesospheric Sounder ISAMS (Global Change Master Directory, 2007), the Halogen Occultation Experiment HALOE (Hervig and Deshler, 2002), and the Atmospheric Chemistry Experiment ACE (Bernath, 2002)) or volume mixing ratio (the Limb Infrared Monitor of the Stratosphere LIMS (NASA, 2007)), which exploit the fact that clouds introduce increased radiance and extinction, but decreased transmission and a decrease in certain specific constituent volume mixing ratios, such as ozone;
- *discontinuity in:* vertical gradients of extinction (the HALOE, or of trace gas concentrations such as ozone (the LIMS), which are introduced by large gradients at the cloud top; and

– *contrast in spectral structure*: (the Cryogenic Infrared Spectrometers and Telescopes for the Atmosphere CRISTA (Spang et al., 2004) or MIPAS (operational method as in Spang et al. (2004), and alternate method presented in Hurley et al. (2009)), which rely upon spectral differences introduced by cloud as opposed to those present in cloud-free spectra.

5 The act of detection yields cursory information on cloud frequency of occurrence and a preliminary measure of cloud top height. In terms of other retrieved cloud parameters, it should be noted that of the instruments discussed ACE, ATMOS, CLAES, HALOE, HIRDLS, and ISAMS operationally retrieve(d) extinction.

1.3 Cloud Information from MIPAS

10 There have been several attempts to retrieve cloud parameters from MIPAS spectra. Firstly, the Monte Carlo Cloud Scattering Forward Model (McCloudsFM) is a multi-scattering model developed by Ewen (2005) to accurately model IR limb emission measurements of cirrus clouds, parameterised by effective radius, number density, cloud top height and cloud depth; however, the computational time associated with the retrieval was prohibitively large, and could not be
15 justified given assumptions made in scattering properties and a priori biases. Secondly, the Earth Observation Science Group at the University of Leicester produces near-real-time cloud top heights from MIPAS spectra from May 2008 onwards (Moore, 2008). The cloud top heights are retrieved using the operational cloud detection method called the Colour Index (CI) Method (Spang, 2004) such that the amount of cloud occurring in a given FOV is roughly anti-correlated
20 with the value of CI. Leicester simply reports the tangent altitude at which cloud is first encountered in the MIPAS scan pattern as the cloud top height. Finally, the Karlsruhe Optimised and Precise Radiative transfer Algorithm (KOPRA) provides accurate simulations of single-scattering clouds in a horizontally symmetric atmosphere, specific to MIPAS. KOPRA has been used to simulate different cloud types, such as cirrus, liquid water clouds, and various types of
25 PSCs — and thus can be used to retrieve the modelled microphysical properties (IMK, 2008) under certain circumstances.

To this end a more comprehensive and operational cloud parameter retrieval algorithm spe-

cific to MIPAS has been developed — and has been adopted as the macrophysical cloud parameter retrieval of the ‘MIPclouds’ project (e.g. Spang et al., 2008). In this work, a non-scattering forward model of the radiation emitted by a cloud in the MIPAS FOV is described, in terms of three macrophysical parameters: cloud top height, top temperature and extinction coefficient corresponding to the limb path, which is dominated by the extinction of the cloud itself. The inverse problem is addressed using an adaptation of standard retrieval theory: a sequential retrieval in which the first guess and a priori are chosen using an estimate of cloud amount.

2 Algorithm Description

The retrieval of macrophysical parameters from a set of MIPAS spectra constituting a single limb-scan is a three-stage process applied independently in different spectral intervals (‘microwindows’). These stages are:

1. Isolating the continuum radiance from each spectrum;
2. Retrieving the Cloud Effective Fraction to locate the spectrum containing the cloud-top; and
3. Retrieving the macrophysical parameters from this and vertically adjacent spectra within the limb scan pattern.

The results from each microwindow are combined to produce a best estimate of the parameters, and an associated error covariance.

2.1 Microwindows

Microwindows (MWs) are small subsets of the MIPAS spectrum of a few wavenumbers in width. A set of ten MWs have been selected in the atmospheric region of $930\text{--}960\text{ cm}^{-1}$ (Table 1) using a modification of the MIPAS MW selection algorithm (Dudhia et al., 2002) optimised for a joint retrieval of continuum and temperature. Fig. 1 shows the positions of these

Table 1. Microwindows for cloud macrophysical parameter retrievals from MIPAS spectra, ordered in terms of priority of selection. Note that the boundaries are multiples of 0.125 cm^{-1} so are consistent with both the ‘full-resolution’ (0.025 cm^{-1} grid) and ‘optimised-resolution’ (0.0625 cm^{-1} grid) spectra. table

| <i>MW#</i> | <i>Wavenumber Range [cm^{-1}]</i> |
|------------|---|
| 1 | 937.625 – 940.625 |
| 2 | 941.125 – 944.125 |
| 3 | 944.500 – 947.500 |
| 4 | 955.750 – 958.750 |
| 5 | 948.625 – 951.125 |
| 6 | 936.000 – 937.625 |
| 7 | 934.500 – 935.875 |
| 8 | 953.500 – 955.000 |
| 9 | 951.875 – 953.250 |
| 10 | 958.750 – 960.875 |

microwindows relative to molecular emission features. Note that each microwindow contains CO_2 lines (for the temperature retrieval, discussed further in Sec. 2.3) whilst avoiding significant contributions from more variable gases such as H_2O .

2.2 Continuum Radiance

5 Using pre-computed molecular transmittance spectra, τ_ν , for each altitude (based on climatological concentrations, and calculated using the radiative transfer model, the Reference Forward Model (RFM) (Dudhia, 2005)) it is possible to identify spectral points where molecular contributions are expected to be negligible (e.g. where $\tau_\nu > 0.95$). It should be noted that at these wavenumbers molecular scattering is also negligible.

10 The continuum radiance, R , and associated error, can then be established by a simple mean and standard error (i.e. using standard deviation D such that the standard error is defined as $D/\sqrt{(n-1)}$, where n is the number of points averaged). By assigning an error value based

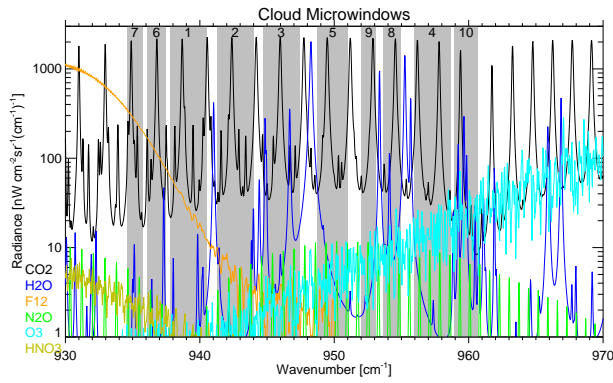


Fig. 1. Modelled full-resolution MIPAS spectrum for a tangent height of 9 km separated by constituent major emitters, in the spectral region of selected MWs listed in Table 1— with MW spectral regions shaded.

figure

on the actual D rather than the instrument noise, some allowance is made for any residual molecular contributions.

2.3 Cloud Effective Fraction

The next step is to identify the spectrum containing the cloud-top. One approach could be to use a simple threshold value on the continuum radiance, but since the continuum radiance is a strong function of atmospheric temperature and atmospheric water vapour content as well as cloudiness, finding a suitable threshold value is difficult. The standard MIPAS Cloud Index (CI) method (Spang et al., 2004) attempts to overcome this temperature dependence by taking the ratio of radiance in two spectral regions ($792 - 796 \text{ cm}^{-1}$ and $832 - 834 \text{ cm}^{-1}$) which react differently to cloud presence. The physical basis of the CI method is that as the field-of-view

(FOV) reaches the limit of being geometrically-fully-filled with opaque cloud, the CI $\rightarrow 1$ (as the cloud continuum radiance overwhelms the gaseous contribution to the spectral signature) whereas in the cloud-free limit, CI is large. Here, instead, it is preferable to have a scheme dependent upon the continuum radiance within each MW independently, as well as one having a more physical basis. This is done via retrieval of a ‘Cloud Effective Fraction’ (CEF) — a parameter first introduced by Hurley et al. (2009).

The CEF is defined as the fraction of the FOV covered by an optically thick, isothermal cloud with a horizontal cloud-top that would give the same continuum radiance as the observed cloud, assuming both have the same Cloud Top Temperature (CTT). Thus a single parameter α (the CEF), can be used to describe the infinite range possible of cloud extinctions and spatial distributions within the actual FOV (although the concept of a single well-defined CTT in all such cases is questionable). Thus α varies from 0 (cloud-free) to 1 (thick cloud completely filling the FOV) with intermediate values which may correspond either to thick cloud filling a small part of the FOV or thin cloud filling a larger fraction.

Mathematically, the CEF, α , for a FOV having central tangent height z_t is defined as

$$\alpha = \frac{\int_{-d}^{z_t - z_c} (1 - e^{-k_c s(z)}) \phi(z) dz}{\int_{-d}^d \phi(z) dz} \quad (1)$$

whereby the FOV can be described as extending a distance $2d$ in the vertical, z_c is the cloud top height measured upward from the Earth’s surface, k_c is the cloud extinction coefficient along the limb path s , and $\phi(z)$ is the FOV vertical response function. From this, it is trivial to see that, to a good approximation,

$$\alpha = \frac{R_c}{B_c} \quad (2)$$

where R_c is the continuum radiance B_c is the (spectrally averaged) Planck function corresponding to the CTT — and this is the definition of CEF used throughout this work.

To retrieve the CEF from a single microwindow spectrum, it is assumed that the observed radiance can be represented as originating from a homogeneous path with the lower fraction

α corresponding to an optically thick cloud whilst the upper fraction $(1 - \alpha)$ originates from molecular emission features above the cloud but at the same local temperature as the cloud-top. Thus, the spectrally varying radiance R_ν , is approximated as

$$R_\nu = \alpha B_c + (1 - \alpha)B_c(1 - \tau_\nu) \quad (3)$$

5 where τ_ν the same pre-computed (climatological) molecular transmittance used in Section 2.2. **Due to the narrowness of the weighting functions characteristic of limb-viewing instruments, the radiance registered within a FOV can be assumed to originate from the FOV tangent height - and not from higher (and potentially warmer) regions of the atmosphere.** It is further assumed that the same expression will hold for other cloud types and distributions with the FOV parametrised
10 by the same CEF value α .

Although clearly a gross simplification, it can be made more realistic by

- (a) using microwindows containing only CO₂ lines rather than more variable absorbers, in which case the climatological τ_ν is likely to be reasonably accurate;
- (b) limiting the fit to spectral points with relatively high transmittance (e.g. $\tau_\nu > 0.75$), in
15 which case the assumption of molecular emission originating near the cloud top is more likely to be valid.

In practice, this works better if B_c is constrained by a priori information — for instance, by using a temperature climatology. A simple, iterative optimal estimation scheme (similar to Eqn. 4) is run to solve Eqn. (3) for α .

20 The cloud-top is identified as lying in the highest altitude spectrum where $\alpha > 0.1$.

The retrieved value of α is also used as a ‘measurement’ in the macrophysical parameter retrieval itself (Sect. 2.4). In principle, Eqn. 3 also yields an ‘improved’ estimate of B_c but, given the crudeness of this approximation, it is preferred to re-use the original climatological temperature profile.

2.4 Macrophysical Parameter Retrieval

The macrophysical parameters are retrieved using an iterative optimal estimation scheme (Rodgers, 2000):

$$\mathbf{x}_{i+1} = \mathbf{x}_i + (\mathbf{K}_i^T \mathbf{S}_y^{-1} \mathbf{K}_i + \mathbf{S}_a^{-1})^{-1} (\mathbf{K}_i^T \mathbf{S}_y^{-1} (\mathbf{y} - \mathbf{f}_i) - \mathbf{S}_a^{-1} (\mathbf{x}_i - \mathbf{a})) \quad (4)$$

where subscript i denotes the iteration number, \mathbf{x} contains the parameters to be retrieved, \mathbf{y} contains the measurements, \mathbf{f} is the forward model (Sect. 2.5) applied to the current iteration of \mathbf{x} , \mathbf{K} is the Jacobian matrix containing elements $\partial \mathbf{f} / \partial \mathbf{x}$, \mathbf{S}_y is the error covariance matrix of \mathbf{y} , \mathbf{a} is the a priori estimate of \mathbf{x} and \mathbf{S}_a is the error covariance of \mathbf{a} . These components are described in the following sections.

2.4.1 State Vector

The state vector \mathbf{x} contains the parameters to be retrieved, and in this case is defined as

$$\mathbf{x} \equiv \begin{pmatrix} z_c \\ B_c \\ \mu_c \end{pmatrix} \quad (5)$$

where z_c is the cloud-top height (CTH), B_c is the Planck function evaluated at the cloud-top temperature T_c (CTT) at the mid-point of the microwindow, and $\mu_c = \log_{10} k_c$, where k_c is the extinction coefficient (in km^{-1}), which is a measure of the cloud extinction (CEX).

In practice, k_c is the extinction coefficient corresponding to the total extinction along the MIPAS limb path, including contributions from both atmospheric and cloud components of measured signal. However, as discussed in Section 2.1, the MWs in which the cloud properties are derived have been pre-selected such that the atmospheric contributions will be negligible in comparison with the cloud signal, having transmittance greater than 95%. Thus, to good approximation, the retrieved value of k_c will correspond to the extinction of the cloud along the MIPAS limb path.

2.4.2 Measurement Vector

The vector \mathbf{y} , containing the measurements used for the retrieval, is defined as

$$\mathbf{y} \equiv \begin{pmatrix} R_u \\ R_c \\ R_l \\ \alpha \end{pmatrix} \quad (6)$$

where R_c is the continuum radiance (Sect. 2.2) from the FOV containing the cloud-top, having the retrieved cloud effective fraction α , while R_u and R_l are the continuum radiances from the FOVs immediately above and below. The measurement covariance matrix \mathbf{S}_y is diagonal, with variances given by the errors from the continuum radiance and CEF retrieval. Although R_c and α are derived from the same spectrum, the argument is that α depends on the spectral structure whereas R_c is derived from the spectrally flat regions — and hence the two may be regarded as independent.

The radiance R_u from the FOV above the cloud-top is expected to have a value ~ 0 (since the CEF for this FOV will have been retrieved with a value < 0.1 , Sect. 2.3) and serves simply to constrain the retrieval from placing the cloud-top too high. The inclusion of the CEF in the measurement vector is discussed in the next section.

2.4.3 A Priori Information

This scheme essentially attempts to retrieve three macrophysical parameters from two non-zero continuum measurements, R_c and R_l . The usual method for dealing with such under-determined problems is to supply independent a priori information. Due to the spatial inhomogeneity of cloud structures, obtaining useful direct a priori information on any of the three retrieved parameters is impractical — however, there are indirect a priori constraints on the *relationships* between the retrieved parameters.

The first a priori constraint is represented by the CEF and is more conveniently introduced into the measurement vector itself (α in Eqn. 6) rather than in the conventional a priori state

vector \mathbf{a} . This acts as a constraint on the CTH and CEX values, as described in Sect. 2.3.

A second source of a priori information is the background temperature profile (obtained, for example, from climatology or meteorological analysis fields). Assuming this is not significantly perturbed in the presence of clouds, this acts as a constraint on the CTH and CTT, since the cloud-top temperature would be expected to correspond to a point on this profile.

Having identified the spectrum containing the cloud-top, the a priori estimate for the cloud-top height is set as the nominal tangent height for that measurement z_t , and its corresponding uncertainty σ_{z_a} set to ± 1 km (*cf. effective FOV width $\sim \pm 1.5$ km, and it is reasonable that this should envelope the uncertainty in cloud top height, if the cloud detection method is trustworthy*).

For this altitude, the background temperature profile provides an equivalent radiance B_t , and uncertainty σ_{B_t} which is typically equivalent to a temperature uncertainty of ± 10 K. However, uncertainty with which z_t represents the actual cloud-top height, and the variation of radiance with altitude $b = dB/dz$ (see Eqn. 9) also have to be taken into account when calculating the a priori covariance matrix elements.

There is no reasonable a priori estimate for optical thickness so it is just set at a typical mid-range value (e.g. $\mu_a = -2.5$) with a large uncertainty $\sigma_{\mu_a} = \pm 0.5$, to capture the range of extinction for which the cloud forward model (Sect. 2.5) is applicable.

Thus the a priori vector is given by

$$\mathbf{a} = \begin{pmatrix} z_t \\ B_t \\ \mu_a \end{pmatrix} \quad (7)$$

Assuming that the Planck function varies linearly with altitude (Eqn. 9), the covariance is given by

$$\mathbf{S}_a = \begin{pmatrix} \sigma_{z_a}^2 & b^2 \sigma_{z_a}^2 & 0 \\ b^2 \sigma_{z_a}^2 & (\sigma_{B_t}^2 + b^2 \sigma_{z_a}^2) & 0 \\ 0 & 0 & \sigma_{\mu_a}^2 \end{pmatrix} \quad (8)$$

2.5 Cloud Forward Model

The essential assumption within the macrophysical retrieval scheme is that a cloud can be represented as a homogeneous ‘grey’ absorber characterised by just three retrieved parameters (the cloud top height z_c , the cloud-top temperature T_c and the cloud extinction k_c).

In addition, it is assumed that the Planck function (evaluated at the spectral mid-point of the microwindow in question) varies linearly with altitude within the cloud with a known gradient, such that

$$B(z) = B_c + b(z - z_c) \quad (9)$$

where $B_c \equiv B(T_c)$ is the Planck function for the cloud top temperature, and $b = dB/dz$ is the vertical gradient ($b < 0$ in the troposphere, $b > 0$ in the stratosphere), derived from an external (e.g. climatological) estimate of the background atmospheric temperature profile.

The cloud forward model (CFM) **f** calculates the continuum radiance originating from a cloud described by z_c , T_c and k_c , and assumes that there is no spectral variation in absorption or in the Planck function over the limited spectral width of each microwindow.

2.5.1 Pencil-Beams

The continuum radiance L_t of a pencil-beam (i.e. infinitesimal solid-angle) viewing at tangent height z_t within the cloud (i.e. $z_t < z_c$) is given by the standard radiative transfer equation for local thermodynamic equilibrium, assuming no molecular contributions from the atmosphere itself, and no scattering:

$$L_t = \int_s B(s) \frac{d\tau}{ds} ds \quad (10)$$

where $B(s)$ is the Planck function (evaluated at the spectral mid-point of the microwindow) along the path s , and $\tau(s)$ is the transmittance along the path s , given by

$$\tau = \exp(-k_c s). \quad (11)$$

Using simple circular geometry (ignoring refraction and assuming the Earth's radius, $r_e \gg z$), the path distance and altitude relative to the tangent point values are related by

$$(s - s_t)^2 \simeq 2r_e(z - z_t). \quad (12)$$

Eqn. (10) can then be solved to give

$$L_t = \left(B_c + \frac{b}{r_e k_c^2} \right) (1 - \tau) - \left(\frac{b s}{2r_e k_c} \right) (1 + \tau). \quad (13)$$

The appearance of the retrieved parameter k_c in the denominator makes this potentially numerically unstable in the optically-thin limit, so a more computationally robust approximation is preferred, such that

$$L_t \simeq \left(B_c + \frac{2}{3} b(z_t - z_c)\tau \right) (1 - \tau), \quad (14)$$

which agrees with the exact solution in the asymptotic limits of transmittance. In the optically thick limit ($\tau = 0$) cloud effectively just emits from its upper surface and $L_t \rightarrow B_c$, as expected, while in the optically thin limit ($\tau \rightarrow 1$) the emission effectively comes from the point one third of the vertical distance from the tangent point to the cloud-top, $L_t \rightarrow (\frac{1}{3}B_c + \frac{2}{3}B_t)(1 - \tau)$, where $B_t \equiv B(z_t)$ from Eqn. (9).

2.5.2 FOV Convolution

The MIPAS FOV response function is represented by a vertical trapezium with a 4 km base and a 2.8 km top when projected onto the atmospheric limb. With tangent heights spaced at 3 km intervals for the original full-resolution measurements, this gives a small overlap between adjacent measurements, but a much larger overlap for the 1.5 km spacing used in the 'optimised-resolution' measurements employed since 2005.

This FOV function ϕ is sampled at N points (in practice, $N = 9$), which determine the altitudes z_j for which the pencil-beam calculations are performed. The measured continuum

radiance is then represented by a numerical convolution of the pencil-beam radiances at these altitudes (L_{t_j}), such that

$$R = \sum_{j=1}^N a_j L_{t_j} \quad (15)$$

where the coefficients a_j are determined according to the assumption that the FOV response function and the cloud radiance vary linearly between calculated points, but that the radiance varies as a step function in the interval containing the cloud-top.

2.5.3 Cloud Effective Fraction

As mentioned in Sect. 2.4.2, the CEF defined in Eqn. 2 is included in the measurement vector, therefore has to be evaluated by the forward model. Using Eqn. 15

$$\alpha = \frac{\sum_{j=1}^N a_j L_{t_j}}{B_c}. \quad (16)$$

Noting that, for optically thick cloud, $L_t \sim B_c$ (Eqn. 14) for pencil-beams which intersect the cloud, and $L_t = 0$ for pencil-beams above the cloud top, this expression for α effectively just depends on the weights a_j , which depend only on z_t .

2.5.4 Definition of Cloud Forward Model

Thus, the CFM \mathbf{f} is simply Eqn. 15 applied to each of the FOVs available in the measurement vector \mathbf{y} , along with the definition of the CEF, α , given in Eqn. 16. Furthermore, since these are analytic expressions, analytic derivatives are used to calculate elements of the Jacobian matrix \mathbf{K} .

2.5.5 Limitations of Cloud Forward Model

As a basic assumption of the forward model (CFM), the modelled cloud is assumed to fully-fill the horizontal domain of the FOV (which is a realistic assumption for cirrus fields, although

potentially not for individual clouds or lower cloud layers) and to extend downwards to the surface of the Earth from the modelled cloud top height. Obviously no cloud will actually extend vertically in such a manner — this assumption is simply taken so that the cloud fills the modelled FOV to the bottom of the FOV below which that in which the cloud top is identified, and since the FOV integration does not consider any pencil-beam radiance contributions beyond this, the effective cloud base is that of the lowest extent of that FOV. These assumptions have implications upon the retrieved parameters:

1. Optically-thin clouds contains good information on all three macrophysical cloud parameters discussed here — but particularly on CEX. However, in this case there is some sensitivity to the FOV-filling assumptions.

– Horizontal Filling Assumption: If, in reality, the cloud does not fully fill the horizontal extent of the FOV (as assumed), the retrieved CEX will be less than the real cloud extinction value. Without further information (for example, imaging to show the horizontal extent of the cloud with respect to the measurement FOV), this remains an untractable problem.

– Vertical Filling Assumption: Similarly, if the cloud does not extend vertically to the bottom of the lowest FOV considered in the CFM (ie. that immediately below the FOV in which the cloud top is identified), a similar effect will be noticed. However, this effect should be minimised because at these wavelengths most clouds should be opaque to radiation higher than the cloud base.

2. Optically-thick clouds will have good information on cloud top height and temperature, but will not be sensitive to extinction. Assumptions on the relative filling of the FOV will not affect the retrieved values of CTH and CTT, and the value of CEX will be fairly arbitrary, having a value reflecting a opaque or near-opaque cloud.

Furthermore, it is worth briefly considering the optical thickness range over which the forward model is applicable. Consider first an optically thin cloud which completely fills the FOV.

From the CFM, it follows that the total radiance in the FOV is

$$R_c = B_c \left(1 - e^{-k_c s}\right) \simeq B_c k_c s \quad (17)$$

The CEF of this thin cloud is

$$\alpha = \frac{R_c}{B_c} \simeq k_c s. \quad (18)$$

5 Assuming a pathlength of approximately 300 km, and that clouds are detected only for $\alpha > 0.1$, this implies that the thinnest cloud which can be registered using this detection method has an extinction coefficient of 0.0003 km^{-1} . Furthermore, for clouds having extinction of the order of 10^{-5} km^{-1} , scattering becomes a non-negligible process, and the CFM is not sufficient to describe the emitted radiance.

10 Turning to the optically thick limit, assume that the extinction is indistinguishable from infinity for path transmittances less than 1%:

$$\tau = e^{-k_c s} = 0.01 \quad (19)$$

Given an estimated pathlength of 300 km, this yields that clouds with $k_c > 0.015 \text{ km}^{-1}$ are indistinguishable from one another.

15 Therefore, it is reasonable to expect that extinction can be retrieved in the approximate range of $-4 \leq \mu_c \leq -1$.

2.6 Combining Microwindow Results

2.6.1 Statistical Combination

20 Retrievals, \mathbf{x}_k , and associated covariances, \mathbf{S}_{xk} , are obtained from each of the $M = 10$ microwindows. These results can then be combined using the standard statistical procedure for independent estimates, such that

$$\hat{\mathbf{S}}_x^{-1} = \sum_{k=1}^M (\mathbf{S}_{xk})^{-1} \quad (20)$$

$$\hat{\mathbf{x}} = \hat{\mathbf{S}}_x \sum_{k=1}^M (\mathbf{S}_{xk})^{-1} \mathbf{x}_k \quad (21)$$

where $\hat{\mathbf{x}}$ and $\hat{\mathbf{S}}_x$ represent the combined estimate and its covariance. There is an assumption here that the retrieved parameters do not vary spectrally — at least across the tens of wavenumbers represented by the selected microwindows (cloud-top radiances are converted to cloud-top temperatures prior to the combination). Extinction, of course, does vary spectrally — however over the small spectral range sampled by the MWs, this variation is not great. It also ignores the fact that the same a priori temperature climatology is used for each estimate, so the separate microwindow results are not strictly independent.

2.6.2 Spike Tests

This combination step also allows a spike-test to be applied — that is, a removal of results from any microwindows which deviate significantly from the mean. The χ^2 statistic is computed for each microwindow individually

$$\chi_k^2 = (\mathbf{x}_k - \hat{\mathbf{x}})^T \hat{\mathbf{S}}_x^{-1} (\mathbf{x}_k - \hat{\mathbf{x}}), \quad (22)$$

and if the microwindow with the highest χ^2 value exceeds the average χ^2 by some factor (e.g. 2) its results are removed from the combination and the test repeated for the remaining microwindows.

2.6.3 Error Inflation

In theory, the covariance $\hat{\mathbf{S}}_x$ should contain the random error information on the retrieved values. However, it is recognised that this is an optimistic assumption since it makes no allowance for the forward model errors or approximations. If the different microwindows produce a large scatter of results, then the standard deviation D of this distribution is likely to be a better estimate of the actual uncertainty, although this does not necessarily allow for forward model errors either since all microwindows make the same assumptions. A three-element vector of

scale-factors \mathbf{e} is constructed to take the maximum of these (in order to conservatively estimate the largest error likely to propagate through from the individual retrievals, rather than the mean of all the individual retrieved errors), such that

$$e_m = \max\left(1, \frac{D_m}{\sigma_m}\right) \quad (23)$$

5 where σ_m is the square root of diagonal element mm in the matrix $\hat{\mathbf{S}}_x$ (i.e. the uncertainty in parameter x_m according to the covariance matrix) and D_m is the actual standard deviation of the parameter x_m from the different microwindow results.

The retrieval covariance is then ‘inflated’ to produce the final covariance, such that

$$\hat{\mathbf{S}}'_{x\ mm} = \mathbf{e}_m^2 \hat{\mathbf{S}}_{x\ mm}. \quad (24)$$

10 2.7 Operational Considerations

The retrieval scheme described attempts to extract the maximum cloud information (i.e. three parameters) from the spectra, and assumes that continuum radiances from the FOV containing the cloud-top, as well as the FOV immediately below, are available (R_c and R_l).

15 In an operational processor, it is desirable to have alternative schemes available to perhaps retrieve fewer parameters in situations where the full retrieval fails (due to an insufficient number of microwindows providing retrievals which converge or pass the spike test), or if insufficient measurements are available (most commonly when the cloud-top is detected in the lowest spectrum in the limb scan).

20 Assuming that a cloud-top has been detected somewhere in the scan, the operational algorithm attempts the following retrieval schemes in sequence until one returns valid results for at least three microwindows.

1. If available, using the measurement from the sweep below the cloud-top R_l (i.e. the cloud-top not located in the lowest sweep in the scan), with a priori extinction information given by $\mu_a = -2.5$ (i.e. mid-range value). This is the full three parameter retrieval (z_c, T_c, μ_c)

from three measurements (R_c, R_l, α) (plus the nominally zero radiance measurement R_u from the sweep above the cloud-top).

2. As (1) but setting $\mu_a = -1.0$, giving a ‘thick cloud’ assumption ($k_c = 0.1 \text{ km}^{-1}$). Such a large initial guess value of extinction reduces the Jacobians with respect to this parameter to nearly zero, effectively leaving just two parameters (z_c, T_c) to be retrieved from three measurements (R_c, R_l, α).
3. As (2) but without R_l — that is, the ‘thick cloud’ assumption allowing for retrieval of two parameters (z_c, T_c) from only one sweep using two measurements (R_c, α). This relies on the CEF retrieval in order to separate the two parameters.

3 Application of Algorithm

This section shows the application of the described retrieval algorithm to a small set of MIPAS data (Section 3.1), in order to highlight the quantities and errors available from the retrieval process itself, without discussion or validation of these results. Section 3.2 discusses the values retrieved by application of the algorithm to a larger MIPAS dataset, comparing to the International Satellite Cloud Climatology Project (ISCCP) high cloud climatology (ISCCP, 2008).

3.1 Example Results: 1 April 2003

In this section, all measurements registered by MIPAS on 1 April 2003 have been processed using the described algorithm to highlight the products calculated and available for further analysis. Fig 2 shows the retrieved values of CTH, CTT and CEX, along with the errors stemming from the retrieval process itself (from the retrieval error covariance matrix). Furthermore, the types of retrieval, as discussed in Section 2.7, are identified by different symbols — and profiles in which there is deemed to be no cloud present are identified by a cross, giving an indication of the proportion of vertical scans taken through the atmosphere having cloud present somewhere in the scan.

3.2 Application and Preliminary Validation of Algorithm to a Test Month: April 2003

Having introduced the products available from application of the retrieval algorithm to MIPAS data, the algorithm is used to process a larger dataset in order to assess whether it provides sensible estimates of cloud properties, and to compare with current climatologies.

5 A full month's data taken in April 2003 is used as a test ensemble. Typically around 25% of sampled MIPAS scan profiles are cloud free throughout the atmosphere, about 40% of vertical scans are retrieved with the full Type 1 retrieval, whilst about 25% are retrieved with the Type 2 retrieval and about 10% with the Type 3 retrieval. The proportion of unsuccessful retrievals is less than 1%.

10 Preliminary validation is carried out qualitatively, by comparing results with the ISCCP high-cloud climatology from the D1 cloud product (ISCCP, 2008) because ISCCP is arguably the most frequently referenced cloud climatology. The high-cloud product calculated by ISCCP is used because only the highest cloud deck at each geographical location sampled by MIPAS is processed, as MIPAS is unable to see below this first-encountered-cloud. ISCCP cloud products are available every three hours — and so average cloud properties over the month are estimated by considering only those data for which there is said to be cloud (ie. no-cloud, clear-atmosphere cases do not enter into the presented averaged products), and averaging in 2.5° x 2.5° latitude/longitude gridboxes. The same process is used to estimate the average cloud properties retrieved from MIPAS, although there are fewer measurements in most latitude/longitude gridboxes due to lower spatial coverage provided by MIPAS).

20 It should be noted that ISCCP infrared cloud products are determined from nadir-measurements — as opposed to the limb-measurements registered by MIPAS — which introduces inherent geometrical differences between the two analyses. Due to the differences in geometry, it is expected that the ISCCP cloud products will show lower cloud top heights (and correspondingly, higher cloud top temperatures) because nadir measurements will penetrate further vertically into clouds, given the same opacity of cloud along the measured vertical-nadir path, than will the limb slant-paths). As well, ISCCP has a much better horizontal resolution when compared with MIPAS (a result of its nadir geometry) so it is possible that ISCCP may be able to detect low

clouds near to high clouds which MIPAS would miss, thus potentially biasing the averaging statistics further.

In addition to geometrical differences between the two, the detection methods used by the two algorithms to identify those measurements in which cloud is said to occur will introduce discrepancies in the cloud products derived, since the sample of clouds selected by both is likely to be different (see ISCCP (2006) for details on ISCCP algorithms). In particular, the ISCCP cloud climatology is known to miss much high, thin cloud (Wylie, 2005), whereas MIPAS is asserted to be more sensitive to thin cloud (as a limb-viewing instrument, e.g. Hurley et al. (2009)).

Finally, ISCCP does not report extinction values, but rather optical depths corresponding to its nadir path, so these can really only be utilised to judge qualitatively what opacity clouds occur where.

Fig 3 shows the results of application of this retrieval algorithm to MIPAS data, along with ISCCP data, from April 2003.

It is immediately obvious that (and most likely as a result of the chosen cloud detection method) the macrophysical cloud parameter retrieval presented here provides information on higher clouds (such as cirrus) which ISCCP appears to miss. MIPAS shows cloud top heights increasing toward the equator, which is expected due to increasing tropopause height toward the tropics, as does ISCCP although not showing such a strong trend. It seems to detect cloud approximately 5-10 km lower than MIPAS, and it is likely that ISCCP predominately misses the high cloud, as either a result of its cloud detection method, or its nadir-geometry, or reassigns the same high cloud a lower cloud top height due to deeper penetration into the cloud itself. Furthermore, ISCCP reports unreasonably high cloud tops at the south pole, as it is improbable that polar stratospheric cloud activity has commenced by such an early date (April) in the calendar year.

Cloud top temperatures are largely anti-correlated with cloud top heights in both the MIPAS and ISCCP results, as expected. Both the ISCCP climatology and the sample of MIPAS retrieved values exhibit the same basic shape with respect to latitude, although those estimated from MIPAS measurements are far colder, corresponding to the far higher cloud top heights

insinuated by MIPAS.

Comparison of cloud opacities is only possible for those MIPAS retrievals for which a full three-parameter retrieval (type 1) is possible. It is worth noting that the CFM is applicable only for clouds having extinction coefficients ranging between 10^{-4} km^{-1} and 10^{-1} km^{-1} , as optically thinner clouds are not detected by the CEF detection method and in any case are dominated by scattering from cloud particles, and thicker clouds have no sensitivity to extinction, as all appear black beyond 10^{-1} km^{-1} . MIPAS seems to see — and appears to retrieve — more thin cloud than do its contemporaries, and particularly in regions such as the tropics where optically-thin cirrus is ubiquitous. Typical values of extinction for cirrus are reported as about $0.05 - 250 \text{ km}^{-1}$, putting the values of extinction retrieved from MIPAS at the lower limit of those currently catalogued. ISCCP products, as representative nadir instrument products, are limited in sensitivity to cloud opacities larger than 0.01, which may indicate that the current climatologies, as derived from predominately nadir instruments, simply bias toward thick cloud as they are unable to capture thin cloud. If this is the case, these extinction results highlight again the suitability of limb-sounding instruments such as MIPAS for cloud analysis and study of thin clouds such as cirrus.

It must be mentioned, however, that the assumptions of horizontally fully-filled FOVs, as well as of cloud bases extending below the bottom of the FOV immediately below that in which the cloud top is located, could also result in low retrieved extinction values for measurements not satisfying these assumptions. There is no way, barring use of some form of added geometrical information (such as coupling imaging of each cloud-field of interest), to avoid this, as there are infinite non-homogeneous arrangements of clouds of varying opacity and clear atmosphere within each FOV. Perhaps in compiling a rigorous cloud climatology, it stands to carefully combine with such extra information in order to ensure that the clear-atmosphere component is kept to a minimum, although this is attempted in this work by choice of suitable MWs of high transmittance.

As well, analysis of the retrieved errors stemming from the retrieval process, as available through the retrieval covariance matrix \mathbf{S}_x , gives a quantitative estimate of the quality of the retrieved results. Fig. 4 shows the distribution of the retrieval errors for the month's worth of

MIPAS data. Generally, the errors due to the retrieval indicate that the forward model/inversion are able to estimate the cloud top height within 50 m, cloud top temperature within 0.5 K, and extinction along the limb path (and largely attributable to the cloud) to within 15% within the range of applicability of $10^{-4} - 10^{-1} \text{ km}^{-1}$.

5 3.3 Validation of Errors using KOPRA Simulations

In practice, however, the real errors are a result of the assumptions made in the forward model — horizontal and vertical (below the cloud top) homogeneity — stemming from insufficiencies in the forward model in describing reality, which cannot truly be evaluated with real MIPAS data. Furthermore, pointing errors will make MIPAS tangent altitudes uncertain by several hundred metres — and will affect the retrieved cloud top heights by the same amount — which is of the order of retrieved errors in CTH.

Whilst the forward model (CFM) discussed in the past few sections well describes an optically grey cloud, it is not necessarily a good representation of real clouds, which scatter radiation in and out of the line-of-sight. It is a useful exercise to compare the CFM with a more realistic model, which allows for scattering — and then to see how well the current retrieval is able to accurately retrieve the macroscopic parameters of a more realistic cloud.

To this end, the Karlsruhe Optimised and Precise Radiative transfer Algorithm (KOPRA) is introduced to provide more accurate simulations of scattering clouds, using a layer-by-layer approach of homogeneous layers in which the radiative transfer proceeds through a succession of extinctions, emissions and scatterings, as described in Höpfner and Emde (2005). KOPRA has been used in the European Space Agency ‘Cloud Information Retrieval from MIPAS Measurements’ MIPclouds study (Spang et al., 2008) to create a cloud spectral database for Polar Stratospheric Clouds, cirrus and liquid water clouds for a wide range of macro- and micro-physical cloud parameters, including atmospheric contributions as well as those resulting from the cloud presence itself.

For the purposes of this exercise, mid-latitude cirrus cases from the database will be considered, as they form the majority of high clouds detected by MIPAS. Mid-latitudinal cirrus has been modelled here as having a cloud top height between 6.5 km and 12.5 km, a cloud depth

between 0.5 km and 4 km, an effective radius between 4.0 μm and 90.0 μm , volume density between 1.1 m^{-3} and $1.1 \times 10^7 \text{ m}^{-3}$, ice water content between $10.0^{-6} \text{ g m}^{-3}$ and 1.0 g m^{-3} , with microphysical parameters defined by Baran (2001). This results in clouds modelled with extinction coefficients between approximately 10^{-5} km^{-1} and 10^2 km^{-1} .

5 For the sake of argument, only KOPRA simulations with cloud top heights of 10.5 km and 11.5 km and cloud depths of 4.0 km are considered (even though for the 11.5 km case the lower FOV will not have the bottom 500 m cloud-filled, but this represents a negligible radiance discrepancy). Fig. 5 compares the radiances coming from KOPRA-simulated clouds and those calculated by the CFM presented here, for the considered cases, with extinction coefficients used to colour-code the different cases.

10 Given that the CFM seems to accurately represent single-scattering clouds as modelled by KOPRA, it is interesting to see how well the macroscopic retrieval can estimate the retrieved parameters, applying the full three-parameter type retrieval. Since KOPRA is a physically more rigorous model, this should give a metric of the skill with which the retrieval can determine cloud parameters for real clouds of various optical thicknesses. Again, considering the mid-latitude cirrus spectra used in the MIPclouds study, the macroscopic retrieval has been run to this end, the results of which are shown in Fig. 6.

15 It appears that the retrieval does a fairly consistent job of determining extinction, especially at lower extinction values ($< 10^{-2} \text{ km}^{-1}$). The retrieval recognises cases of higher extinction as such — but does not necessarily get the extinction coefficient quite right for high cloud extinction, since there are negligible radiance differences once the cloud approaches the opaque limit, from values of 10^{-2} – 10^{-1} km^{-1} .

20 In terms of the retrieved cloud top heights and cloud top temperatures, the retrieval tends to consistently retrieve within 50 m and 0.5 K — however for cases of high cloud effective fraction (extinctions greater than about 0.1 km^{-1}) it tends to overestimate cloud top height and temperature by up to 250 m and 5 K, and underestimate the extinction, in an attempt to best match the higher CFM-predicted radiance for these cases.

25 In conclusion, retrievals of KOPRA simulations (which are expected to better represent true clouds as they scatter radiance) using the simple CFM are reliable to within 50 m, 0.5 K and

a factor of 15% of the extinction coefficient. Thus, the CFM and retrieval based upon it work reliably within the design bounds and estimated retrieval errors provided by the error covariance matrix \mathbf{S}_x , well representing clouds for which scattering is not dominant.

3.4 Water Vapour Continuum

At altitudes sampled by the lower tangent heights in the vertical MIPAS scan pattern (e.g. those less than about 6 km), the water vapour continuum is difficult to distinguish from the continuum radiance introduced by emitting clouds. Due to this difficulty, the water vapour continuum becomes a potential issue for reliable cloud detection, and for retrieval of accurate cloud properties. It is possible that the water vapour spectral lines contained within some of the selected MWs could be used to characterise the concentration of water vapour locally in the atmosphere (at tangent heights immediately above that identified as containing the cloud top), which could then be used to disentangle the effects of the water vapour continuum from the cloud signal. In the current algorithm, the absorption from the water vapour continuum is taken into account to some extent in the utilised molecular transmittance spectra, whereby the expected water vapour continuum is effectively ‘subtracted’ from the measured continuum to establish the cloud contribution.

This has not been studied in this work, although it warrants further study, and as such may introduce errors in application of the algorithm as currently described, as regions of large water vapour concentration could be erroneously selected as cloudy measurements.

3.5 Comparison of CEF and CI Detection Mechanisms

Section 2.3 describes the method used to select measurements as containing cloud and as the CI Method is the traditionally used method, this section seeks to assert that the CEF is reasonable as a cloud detection method, and in fact, may capture more optically-or-geometrically thin cloud. In this section, application of both CEF and CI cloud detection methods to the same set of spectra. This set of spectra is selected as all those spectra measured below 30 km above which the CEF method first detects a cloud top, which will give a realistic selection of clear

and cloudy examples. Comparison between the two detection mechanisms is made using real MIPAS data for all measurements registered on 1 April 2003.

Fig. 7 shows the results of this comparison, highlighting that the CEF scheme detects more cloud than does the CI method **with the application of the operational CI threshold of 1.8 (which, arguably is set to detect clouds sufficiently opaque to cause problems for trace gas retrievals) and CEF threshold of 0.1**. It is plausible that the scatter of points at higher CI are indeed cloudy cases, as there appears to be larger scatter than attributable to normal variations of temperature and trace-species concentrations. Furthermore, if the thresholds are applied and cloud detection is carried out, the CEF scheme detects more cloud particularly in regions where thin cloud such as polar stratospheric clouds or cirrus are expected. In general, the CEF method selects far more measurements as cloud-contaminated — which should yield a more complete selection of cloud data upon which to create climatological analysis.

It is worth noting that the percentage of spectra identified as containing cloud is dependent upon the choice of threshold applied to each detection method. For instance, at the operation threshold of 1.8, the CI method detects cloud in 9.8% of the studied set of spectra. The CEF method will select 9.8% of the spectra as containing cloud if its threshold is modified to 0.32 (instead of the suggested 0.1), although it is worth noting that both methods do not choose all the same individual cases as cloud-contaminated. If the CI threshold for cloud is loosened to 4.0, it selects 17.6% of the spectra in the set as cloudy — a percentage which can be matched by setting the CEF threshold to 0.08.

Application of CEF and CI cloud detection methods with the current thresholds, to MIPAS data highlights that the CEF method detects more possible cloud, including thin cloud which is so frequently missed from current cloud climatologies such as ISCCP (ISCCP, 2008).

4 Conclusions

This study confirms that cloud top height, cloud top temperature and extinction coefficient can be successfully retrieved by modelling clouds quite simply and by using an optimal estimation-type retrieval whereby an estimate for CEF initiates the retrieval close to the correct

cost minimum. The retrieval algorithm has been tested and found reliable on simulated data, and compared with the ISCCP climatology when the applied to real MIPAS data. The retrieval errors associated with application of this algorithm to both real and simulated data can be used to determine a measure of confidence for how well the forward model represents realistic scattering clouds. From this, CTH is retrieved to within 50 m, CTT to within 0.5 K and k_c within a factor of 15% for clouds having extinction between 10^{-4} km^{-1} and 10^{-1} km^{-1} , although there do exist cases in which higher error exists. The CTH and CTT retrievals are quite robust, however the CEX retrieval (especially for thin cloud) is sensitive to the assumptions of homogeneity within the FOV, and it is possible that the CEX can be underestimated due to atmospheric contributions along the limb path over which the extinction is calculated, although this effect is hopefully minimised inasmuch as possible by using atmospheric windows of negligible gaseous absorption.

It should be noted that the greatest error is expected to result from the error in the initial forward model assumption of horizontal homogeneity — that is, that a cloud can be represented by a single flat cloud top height, a single extinction coefficient and a consistent temperature structure throughout the body of the cloud. Horizontal homogeneity is a simplification of the geometry and optics of real clouds — but there are infinite possible cloud fields and it is impossible to retrieve inhomogeneous fillings of the MIPAS FOV without prior knowledge of the geometry of the inhomogeneity. Thus, whilst the assumption of horizontal homogeneity is insufficient to fully represent reality, it is the closest representation that can be accomplished without some other a priori knowledge such as a limb imager coinciding with the FTS view.

Acknowledgements. Part of this work was done as part of a DPhil undertaken at the University of Oxford under the funding of the Commonwealth Scholarship Committee in the UK. Part of this work was supported by ESA through the MIPClouds project: ‘Cloud Information Retrieval from MIPAS Measurements’, AO/1-5255/06/I-OL.

References

references

- Barton, I.: Upper-level cloud climatology from an orbiting satellite, *J. Atmos. Sci.*, 40, 435–447, 1983.
- Bernath, P.: The Atmospheric Chemistry Experiment (ACE): An Overview, *Geoscience and Remote Sensing Symposium, IGARSS '02*, 2002.
- CLAES: website on SPASCI CLAES Mission, www.spasci.com/CLAES/mission.html, 2007.
- 5 Dudhia, A.: website on the Reference Forward Model (RFM): Software User's Manual (SUM), <http://www-atm.physics.ox.ac.uk/RFM/sum.html>, 2005.
- Dudhia, A., Jay, V. L., and Rodgers, C. D.: Microwindow selection for high-spectral-resolution sounders, *Appl. Optics*, 41, 3665–3673, 2002.
- European Space Agency: website on ESA ENVISAT, <http://envisat.esa.int/instruments/images/MIPAS\Interferometer.gif>, 2005.
- 10 ESA Living Planet: website, http://www.esa.int/esaLP/SEM/NAT8I77G\LPcampaigns_0.html, 2010.
- Ewen, G.: *Infrared Limb Observations of Cloud*, DPhil thesis in Atmospheric, Oceanic and Planetary Physics, University of Oxford, Oxford, UK, 2005.
- Global Change Master Directory: website on ISAMS, <http://geodiscover.cgdi.ca/gdp/search?action=fullMetadata&entryLang=fr&entryId=5640&entryType=productCollection>, 2007.
- 15 Hervig, M. and Deshler, T.: Evaluation of aerosol measurements from SAGE II, HALOE, and balloon-borne optical particle counters, *J. Geophys. Res.*, 107, AAC3.1–AAC3.12, 2002.
- Höpfner, M. and Emde, C.: Comparison of single and multiple scattering approaches for the simulation of limb-emission observations in the mid-IR, *J. Quant. Spectrosc. Radiat. Transfer*, 1, 275–285, 2005.
- 20 Hurley, J., Dudhia, A., and Grainger, R. G.: Cloud detection for MIPAS using singular vector decomposition, *Atmos. Meas. Tech.*, 2, 533–547, 2009.
- IMK: website on IMK Karlsruhe Optimized and Precise Radiative transfer Algorithm, http://www-imk.fzk.de/asf/ame/publications/kopra_docu/, 2008.
- Intergovernmental Panel on Climate Change: Fourth Assessment Report Climate Change 2007 — The Physical Science Basis, Cambridge University Press, Cambridge, 2008.
- 25 ISCCP: website on ISCCP, <http://isccp.giss.nasa.gov/index.html>, 2008.
- ISCCP: website on ISCCP algorithm description, <http://isccp.giss.nasa.gov/newalg.html>, 2006.
- Kahn, B., Eldering, A., Irion, F., Mills, F., Sen, B., and Gunson, M.: Cloud identification in Atmospheric Trace Molecule Spectroscopy infrared occultation measurement, *Appl. Optics*, 41, 2768–2780, 2002.
- 30 Lambert, A., Bailey, B., Edwards, D., Gille, J., and Johnson, B.: High Resolution Dynamics Limb Sounder Level-2 Algorithm Theoretical Basis Document 2, Tech. rep., 1999.
- Mantovani, R.: ENVISAT MIPAS Report: Mar 2004 - Feb 2005, ENVI-SPPA-EOPG-TN-05-0006, Tech. rep., European Space Agency, 2005.

- Moore, D.: website on University of Leicester Cloud Top Height product, http://www.leos.le.ac.uk/mipas/data/nrt_ci.html, 2008.
- NASA: website on GES Distributed Active Archive Center LIMS User's Guide, <ftp://disc1.sci.gsfc.nasa.gov/data/lims/Documentation/>, 2007.
- 5 Prabhakara, C., Fraser, R., Dalu, G., Wu, M. abd Curran, R., and Styles, T.: Thin cirrus clouds: Seasonal distribution over oceans deduced from NIMBUS-4 IRIS, *J. Appl. Meteor.*, 27, 379–399, 1988.
- Rodgers, C.: *Inverse Methods for Atmospheric Sounding: Theory and Practice*, World Scientific Publishing Co Pte Ltd, 2000.
- SAGE-III-ATBD-Team: SAGE III Algorithm Theoretical Basis Document (ATBD) Cloud Data Products, LaRC 475-00-106, 1.2, Tech. rep., 2002.
- 10 Sayer, A. M., Campmany, E., Dean, S., Ewen, G., Poulsen, C. A., Arnold, C., Thomas, G. E., Grainger, R. G., Siddans, R., Lawrence, B., and Watts, P.: Validation of GRAPE ORAC ATSR-2 cloud products, p. in preparation, 2009.
- Spang, R., Remedios, J., and Barkley, M.: Colour Indices for the Detection and Differentiation of Cloud Types in Infra-red Limb Emission Spectra, *Adv. Space Res.*, 33, 1041–1047, 2004.
- 15 Spang, R., Griessbach, S., Hopfner, M., Dudhia, A., Hurley, J., Siddans, R., Waterfall, A., Remedios, J., and Sembhi, H.: Technical Note: Retrieval of MIPAS cloud parameter, ESA-ITT AO/1-5255/06/I-OL, Tech. rep., European Space Agency, 2008.
- Warren, S., Hahn, C., and London, J.: Simultaneous occurrence of different cloud types, *J. Clim. Appl. Meteor.*, 24, 658–667, 1985.
- 20 Woodbury, G. and McCormick, M.: Global Distributions of Cirrus Clouds Determined from SAGE Data, *Geophys. Res. Lett.*, 10, 1180–1183, 1983.
- Wylie, D. and Menzel, W.: Two years of cloud cover statistics using VAS, *J. Clim. Appl. Meteor.*, 2, 380–392, 1989.
- 25 Wylie, D., Menzel, W., Woolf, H., and Strabala, K.: Four Years of Global Cirrus Cloud Statistics Using HIRS, *J. Climate*, pp. 1972–1986, 1994.
- Wylie, D., Jackson, D., Menzel, W., and Bates, J.: Trends in Global Cloud Cover in Two Decades of HIRS Observations, *J. Climate*, 130, 3021–3033, 2005.

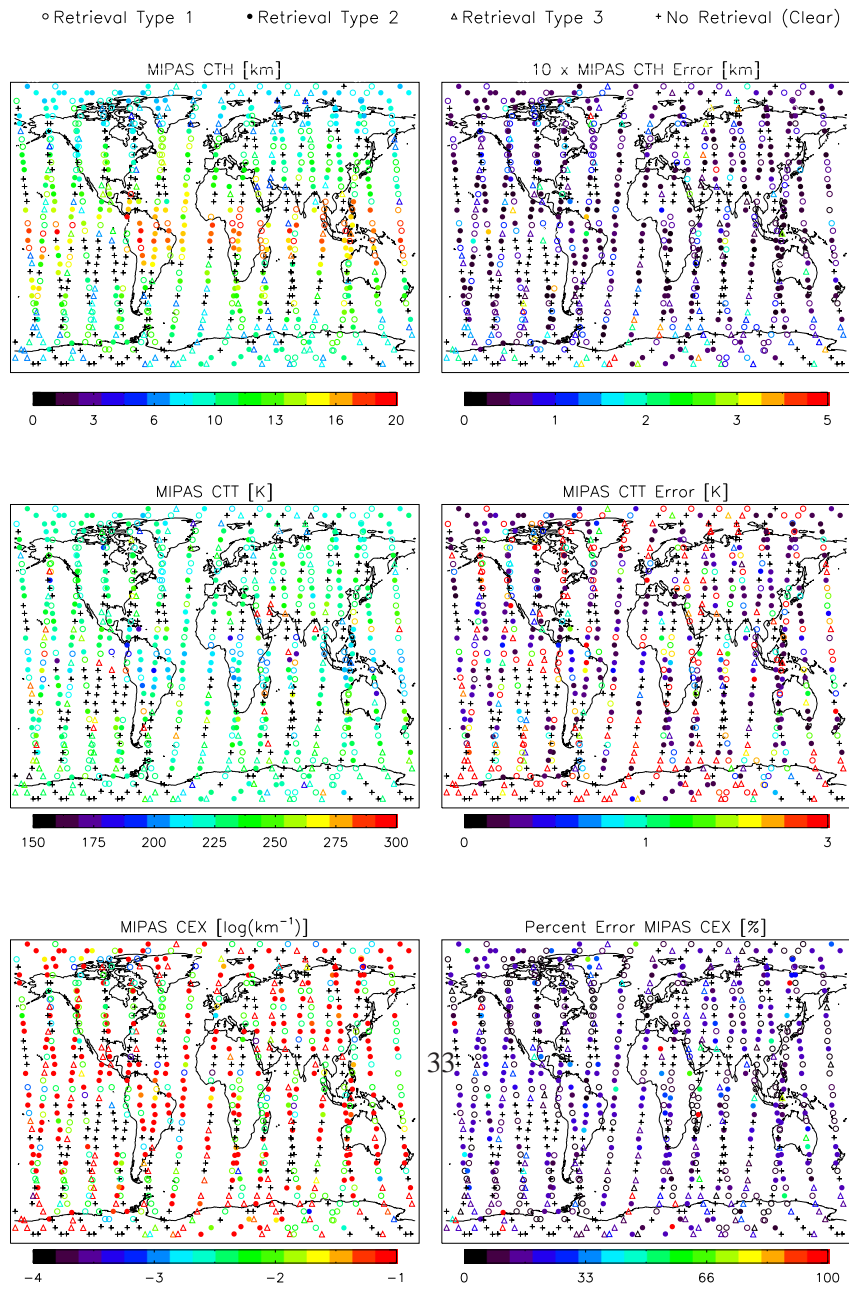


Fig. 2. Application of algorithm to all MIPAS measurements taken on 1 April 2003. Retrieved parameters (left column) of CTH (top panels), CTT (middle panels) and k_c (bottom panels) and errors thereof (right panels) are given, noting the type of retrieval, corresponding to the available measurement FOVs.

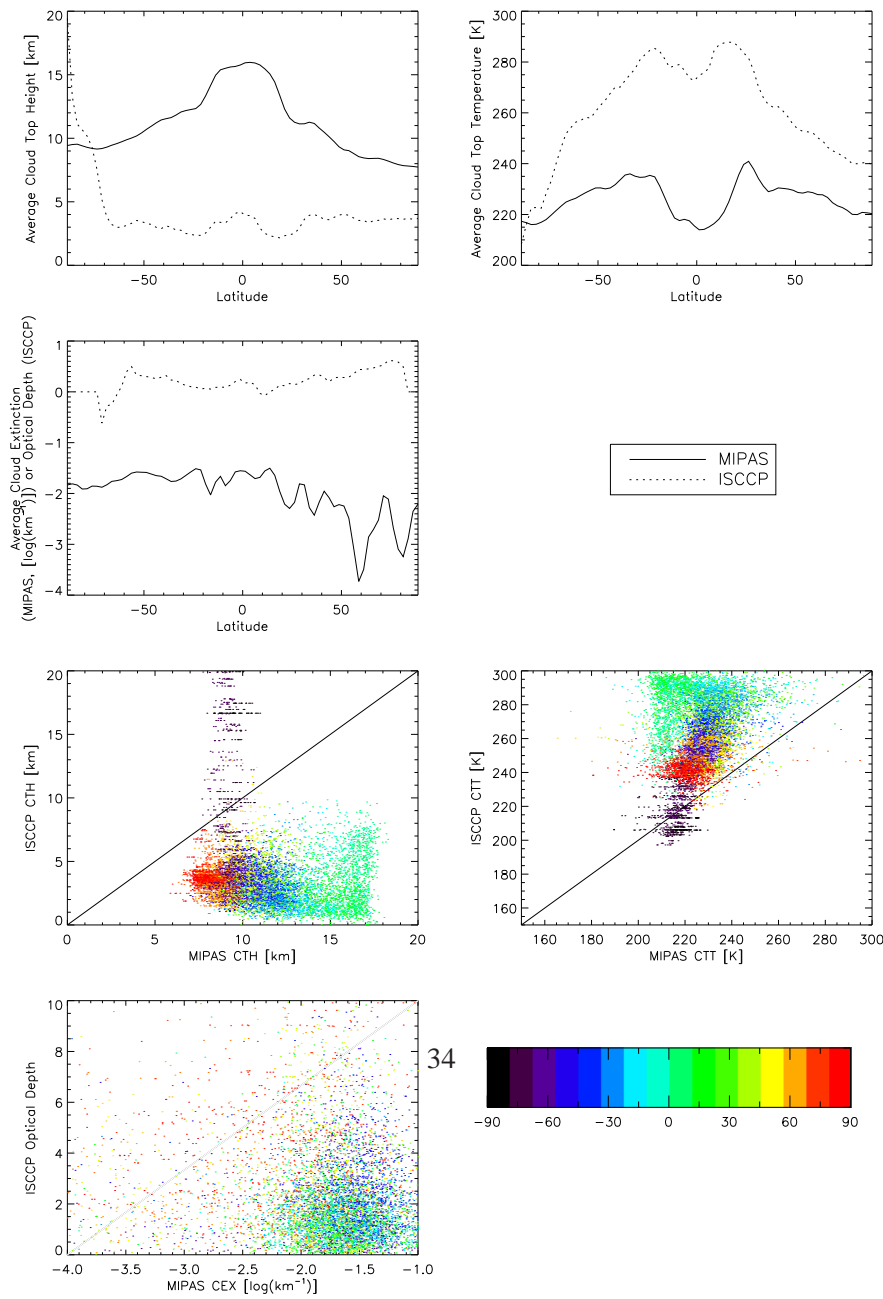


Fig. 3. Top panels: Zonally-averaged retrieved cloud top height (top left), cloud top temperature (top right) and logarithm of extinction coefficient (bottom left) when algorithm is applied to a month's worth of MIPAS data (solid lines), along with corresponding ISCCP quantities (dotted lines). Bottom panels: Scatterplot showing average cloud top height (top left), cloud top temperature (top right) and cloud extinction (bottom left) in a 2.5° by 2.5° latitude/longitude grid for MIPAS and ISCCP. Solid line shows one-to-one limit. Points colour-coded by latitude.

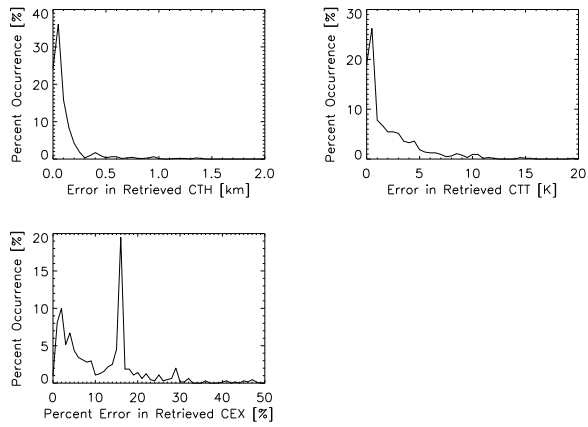


Fig. 4. Retrieval errors for cloud top height (top left), cloud top temperature (top right) and extinction coefficient (bottom) from application of algorithm to all MIPAS measurements taken in April 2003.

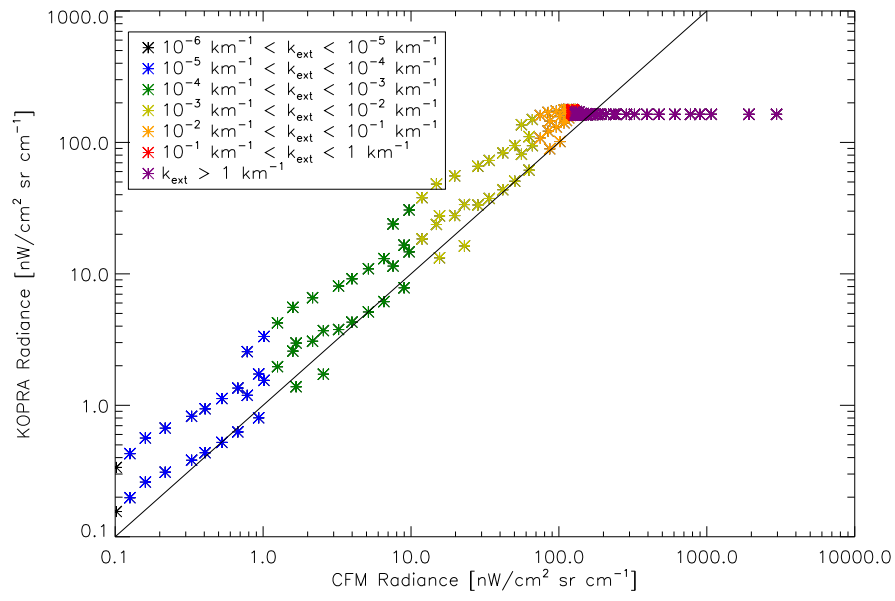


Fig. 5. Comparison of KOPRA (scattering and thus more realistic) and CFM (non-scattering) radiances, as a function of extinction coefficient, as indicated by colour-scale.

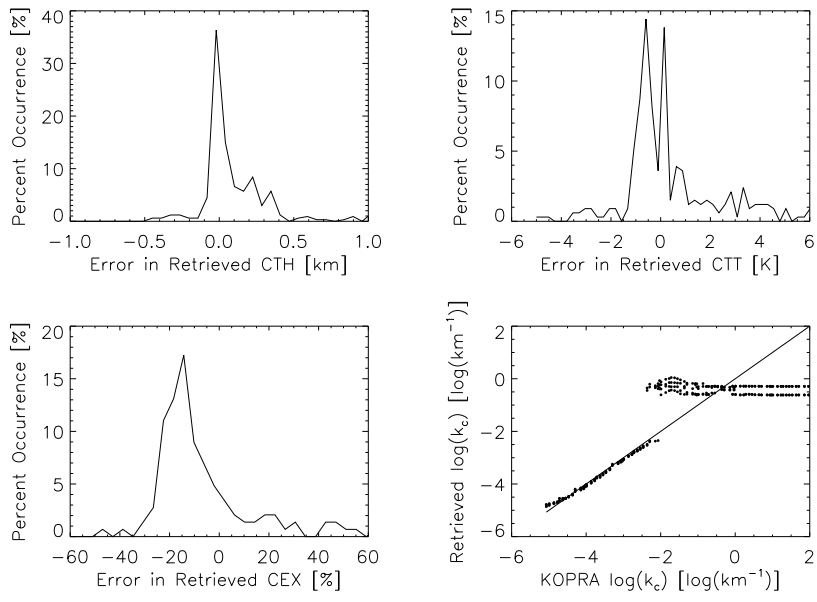


Fig. 6. Top panels: Probability distribution functions of difference between retrieved and simulated CTH (left) and CTT (right) for KOPRA-simulated clouds. Lower left panel: Probability distribution function of the percent relative difference between KOPRA-simulated k_c and retrieved k_c . Lower right panel: Scatterplot of retrieved $\log(k_c)$ (right panel) for KOPRA-simulated clouds. Black line shows one-to-one division.

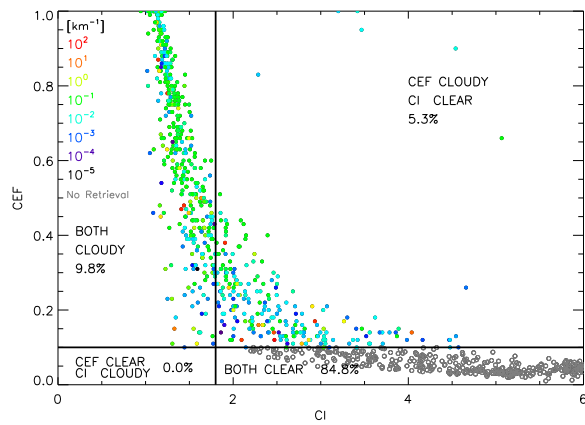


Fig. 7. Correlation between CI and CEF (evaluated in MW1) colour-coded by extinction coefficient (for those cases for which the retrieval has been evaluated) and by open circles for clear scans, for all spectra above the cloud top (if any) measured MIPAS on 1 April 2003. CI is anti-correlated and CEF is correlated with cloud amount. Horizontal line shows the CEF threshold (above which cloud occurs) and vertical line shows the CI threshold (to the left of which cloud occurs).